Volume 16
Number 10
14 March 2024
Pages 4923-5444

Nanoscale

rsc.li/nanoscale

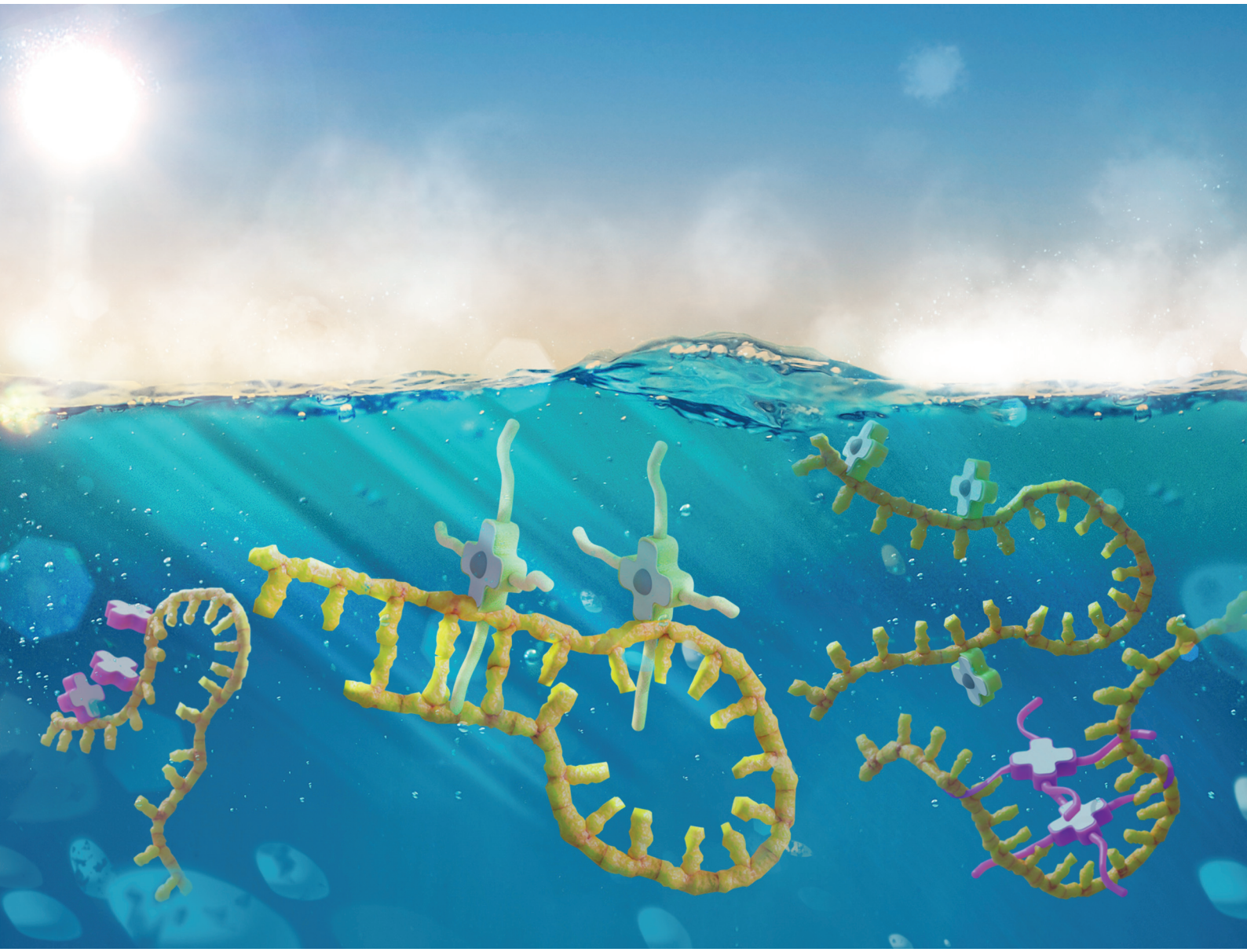

ISSN 2040-3372

ROYAL SOCIETY OF CHEMISTRY

PAPER
Roberto Purrello, Alessandro D'Urso *et al.*
Interactions between achiral porphyrins and a mature miRNA

NCNST

Nanoscale

PAPER

View Article Online
View Journal | View Issue

Cite this: *Nanoscale*, 2024, **16**, 5137

Interactions between achiral porphyrins and a mature miRNA†

Gabriele Travagliante,[a] Massimiliano Gaeta,[a] Chiara M. A. Gangemi,[b] Salvatore Alaimo,[c] Alfredo Ferro,[c] Roberto Purrello *[a] and Alessandro D'Urso *[a]

Recent discoveries have revealed that mature miRNAs could form highly ordered structures similar to aptamers, suggesting diverse functions beyond mRNA recognition and degradation. This study focuses on understanding the secondary structures of human miR-26b-5p (UUCAAGUAAUUCAGGAUAGGU) using circular dichroism (CD) and chiroptical probes; in particular, four achiral porphyrins were utilized to both act as chiroptical probes and influence miRNA thermodynamic stability. Various spectroscopic techniques, including UV-Vis, fluorescence, resonance light scattering (RLS), electronic circular dichroism (ECD), and CD melting, were employed to study their interactions. UV-Vis titration revealed that meso-tetrakis(4-*N*-methylpyridyl) porphyrin (H2T4) and meso-tetrakis(4-carboxyphenylspermine) porphyrin (H2TCPPSpm4) formed complexes with distinct binding stoichiometries up to 6 : 1 and 3 : 1 ratios, respectively, and these results were supported by RLS and fluorescence, while the zinc(II) derivative porphyrin ZnT4 exhibited a weaker interaction. ZnTCPPSpm4 formed aggregates in PBS with higher organization in the presence of miRNA. CD titrations displayed an induced CD signal in the Soret region for every porphyrin investigated, indicating that they can be used as chiroptical probes for miR-26b-5p. Lastly, CD melting experiments revealed that at a 1 : 1 ratio, porphyrins did not significantly affect miRNA stability, except for H2TCPPSpm4. However, at a 3 : 1 ratio, all porphyrins, except ZnTCPPSpm4, exhibited a strong destabilizing effect on miRNA secondary structures. These findings shed light on the structural versatility of miR-26b-5p and highlight the potential of porphyrins as chiroptical probes and modulators of miRNA stability.

Received 31st October 2023,
Accepted 17th January 2024

DOI: 10.1039/d3nr05504c

rsc.li/nanoscale

1. Introduction

MicroRNAs (miRNAs) are a class of highly conserved, short (18–24 nucleotides) and non-coding RNAs that regulate gene expression by base pairing to one or more mRNA targets, causing either target degradation or translational repression.[1] The distinctive miRNA sequences are involved in many physiological and pathological processes. Indeed, miRNAs play important roles in immune response,[2] hematopoiesis, developmental timing, cell death, cell proliferation and patterning of the nervous system[3] and carcinogenesis.[4] Dysregulation of miRNAs contributes to the initiation and development of human diseases like cancer, genetic disorders, cardiovascular diseases and altered immune system functions.[5–7] Recent insight into the roles of miRNAs have made them attractive tools and targets for novel therapeutic approaches.[8] Due to the relevant roles of miRNAs in biological processes connected with cancer, mature miRNA stabilization or destabilization by small molecule ligands could be used as a selective, novel, anti-cancer therapeutic strategy.

Additionally, it has been recently discovered that mature miRNAs could form highly ordered structures similar to aptamers and their structural versatility may determine a variety of functions other than the well-known mechanism of mRNA recognition and degradation. Indeed, miRNAs, like RNA aptamers, could be induced to bind with proteins and hence influence their activity directly, suggesting that miRNA secondary structures may have functions outside of the RISC (RNA-induced silencing complex) in terms of both the sequence and structure.[9–11] However, the biological role of these conformations is still unknown. As a result, identifying the various structures and particular sequences of miRNAs using functional probes capable of interfering with processes governing the biological functions might lead to a better understanding

[a]*Dipartimento di Scienze Chimiche, Università degli Studi di Catania, Viale A. Doria 6, 95125 Catania, Italy. E-mail: rpurrello@unict.it, adurso@unict.it*
[b]*Dipartimento di Scienze chimiche, biologiche, farmaceutiche e ambientali, Università degli Studi di Messina, V.le Ferdinando Stagno d'Alcontres 31, 98166 Messina, Italy*
[c]*Dipartimento di Medicina Clinica e Sperimentale, c/o Dipartimento di Matematica e Informatica, Università degli Studi di Catania, Viale A. Doria 6, 95125 Catania, Italy*

† Electronic supplementary information (ESI) available: All UV, fluorescence, RLS and CD titrations in addition to the detailed description of binding constant determination. See DOI: https://doi.org/10.1039/d3nr05504c

of the mechanisms behind some diseases and the development of new therapies.

Generally, DNA or RNA probes are formed by aromatic chromophores with the potential to intercalate with nucleic bases *via* π–π interactions. Among them, porphyrins appear to be an excellent choice because of their unique properties. In addition to a highly conjugated π electron system leading to an intense absorption band in the 380–450 nm region (the Soret band), they can be functionalized at the meso-positions with cationic groups favoring interactions with anionic phosphates. Finally, when non-chiral peripheral substituents are present, porphyrins are achiral molecules and do not display any chiroptical signal. However, interestingly, after interaction with chiral molecules (such as DNA, RNA, *etc.*), an induced circular dichroism (ICD) signal in the Soret absorption band region could be observed. This signal arises from chiral distortion of the porphyrin symmetry or intermolecular extinction coupling between at least two chiral oriented chromophores.[12] Furthermore, porphyrins' capacity to behave as photosensitizers in the presence of oxygen piqued scientists' interest in examining the binding of porphyrinoids to polynucleic acids in order to employ them in photodynamic therapy (PDT). Although several achiral cationic or anionic porphyrins have been studied as chiroptical probes to investigate the secondary structures of different biomolecules in aqueous solution, such as polynucleotides, oligopeptides, proteins and so forth,[13,14] there is a lack of studies regarding the non-covalent interactions of achiral porphyrins with miRNAs.

However, it is important to mention that mature miRNAs are comparatively shorter than the previously studied nucleic acid sequences. Therefore, the spectroscopic features reported for the binding modes of porphyrins with nucleic acids may serve in the present study as a guide to understand the reciprocal disposition of porphyrins and bases but not necessarily the binding mode. Indeed, to the best of our knowledge, this is the first study on the spectroscopic characterization of porphyrin–miRNA binding modes and appears intriguing for biomedical applications.

In order to investigate whether porphyrins can be used as chiroptical probes and/or modulate the stability of miRNA structures, we studied the interactions between miR-26b-5p and four different porphyrins (Fig. 1).

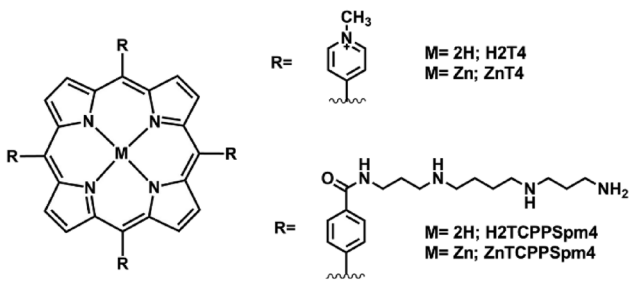

Fig. 1 Structures of H2T4 and H2TCPPSpm4 with their respective Zn(II) derivatives, ZnT4 and ZnTCPPSpm4. For the clarity of the image, the axial water molecule attached to Zn(II) of ZnT4 is not depicted.

The human miR-26b-5p sequence (UUCAAGUAAUUCAGGAUAGGU) has been chosen for its biological relevance. Indeed miR-26b is found in an intron of the Ctdsp2 gene and it acts synergistically with its host gene to regulate neuronal development.[15] It has been revealed that miR-26b is a crucial regulator in carcinogenesis and tumor progression in several forms of cancer by serving as a tumor suppressor gene. This target downregulation represses cellular proliferation in breast cancer[16] and inhibits metastasis of osteosarcoma.[17] Furthermore, a recent study shows that miR-26b-5p inhibits the proliferation, migration, and invasion of intrahepatic cholangiocarcinoma cells *via* inhibiting S100A7.[18] Similarly, downregulation of miR-26b-5p and miR-26a-5p in bladder cancer cells was observed and both of these miRNAs significantly prevented cancer cell motility and invasion.[19,20] Aside from cancer, altered miR-26b expression and functional abnormalities have been identified in a range of different disorders. These findings show that miR-26b plays a role in cardiac function maintenance[21] and it has been found to be elevated in the human temporal cortex in Alzheimer's disease development.[22]

In this work, we first investigated by electronic circular dichroism (ECD) and ECD-melting experiments the possible secondary structures adopted by human miR-26b-5p. Then by UV-vis, fluorescence, resonance light scattering (RLS), ECD and ECD melting, we characterized the interactions between miR-26b-5p and meso-tetrakis(4-*N*-methylpyridyl) porphyrin (H2T4) and its zinc(II) derivative, ZnT4. Under physiological conditions, both porphyrins bring cationic charges in the four meso-positions. In addition, H2T4 is able to intercalate in the DNA GC-rich region *via* stacking interactions with nucleobases.[23] The latter type of interaction is precluded to ZnT4 owing to the penta-coordinated nature of the central Zn, which hinders intercalation.[24,25] Successively, in order to evaluate the role of electrostatic interactions, we studied the interactions of the title miRNA with other two porphyrins bearing four multicationic spermine arms (meso-tetrakis(4-carboxyphenylspermine) porphyrin, H2TCPPSpm4,[26] and its Zn(II) derivative, ZnTCPPSpm4) (Fig. 1). We selected the two sperminated derivatives in order to improve the biocompatibility of porphyrins since it is known that the polyamine transport system of these cells affords a selective accumulation of polyamine analogues in neoplastic tissues.[27] In addition, it has been already shown that H2TCPPSpm4 is able to stabilize G-quadruplex superstructures[28] and it can interact with a variety of DNA structures,[29,30] whereas ZnTCPPSpm4 can detect, catalyze and stabilize Z-DNA.[31]

2. Experimental section

2.1. Materials

The phosphate buffered saline (PBS) tablets were purchased from Sigma-Aldrich Company and the stock solution was prepared by dissolving one tablet in 200 ml of ultrapure water. PBS buffer (pH = 7.4) contains 10 mM phosphate buffer

sodium salt ($[H_2PO_4^-]$ + $[HPO_4^{2-}]$ = 10 mM), 137 mM sodium chloride, and 2.7 mM potassium chloride.

The miR-26b-5p sequence used was purchased from Integrated DNA Technologies IDT® and used without further purification. The solid was dissolved in ultra-pure water obtained from an Elga Purelab Flex system by Veolia with a purity of 18.2 MΩcm, achieving a stock solution with a concentration of ~100 μM. Annealing was performed by increasing the temperature up to 90° for 5 min, then cooling down slowly up to room temperature and finally storing the solution at 4 °C for one night. The concentrations of miR solutions were checked by performing UV-vis measurements at 80 °C using the extinction coefficient of the sequence given by IDT: $\varepsilon_{260\ nm}$ = 224 200 L (mol cm)$^{-1}$; then, by diluting in 10 mM PBS buffer ([KCl] 2.7 mM; [NaCl] 137 mM; pH 7.4), we prepared the sample solution.

ZnT4 porphyrin was obtained by metalation of the naked tetracationic porphyrin (purchased from Mid-Century) following the well-known procedure reported in the literature.[32] The stock solutions of H2T4 and ZnT4 were prepared by dissolving the solid in ultrapure water to achieve concentrations ranging from 3 × 10^{-4} M to 4 × 10^{-4} M. The concentrations of these stock solutions were checked by spectrophotometric experiments using ε_{423} = 224 000 M^{-1} cm^{-1} for H2T4 and ε_{437} = 204 000 M^{-1} cm^{-1} for ZnT4 in water.

H2TCPPSpm4 and ZnTCPPSpm4 were obtained according to the literature procedure.[26,31] All stock solutions of H2TCPPSpm4 were prepared by dissolving the solid in DMSO to avoid the aggregation process, whereas stock solutions of ZnTCPPSpm4 were prepared by dissolving the solid in ultrapure water in order to achieve concentrations ranging from 2 × 10^{-4} M to 3 × 10^{-4} M. The concentrations of these stock solutions were checked by spectrophotometric experiments using ε_{437} = 338 000 M^{-1} cm^{-1} at pH = 1 in HCl water solution for H2TCPPSpm4 and ε_{423} = 133 766 M^{-1} cm^{-1} at pH = 3.5 in HCl water solution for ZnTCPPspm4.

2.2. Electronic circular dichroism

ECD spectra were recorded at 20 °C using a Jasco J-715 spectropolarimeter equipped with a single position Peltier temperature control system. A quartz cuvette with a 1 cm path length was used for all ECD experiments. A solution of 2.5 μM miR-26b-5p was titrated with increasing amounts of porphyrin and CD scans were collected with the following parameters: scanning rate: 50 nm min^{-1}, data pitch: 0.5 nm, digital integration time (D.I.T.): 2 s, and bandwidth: 2.0 nm. Each ECD spectrum was an average of at least five scans. CD melting was performed at porphyrin : miR ratios of 1 : 1 and 3 : 1 respectively, with the following parameters: 260 nm wavelength, 5–90 °C temperature range, 1 °C min^{-1} temperature slope and 8 s response.

CD melting curves were obtained from the experimental data with the help of the Boltzmann sigmoid equation: Y = bottom + (top − bottom)/(1 + e((T_m − x)/slope)), and the Boltzmann sigmoid function was characterized by a bottom, a top plateau, and a characteristic value describing the point where the x value is exactly between the top and bottom values, here T_m (melting temperature).

2.3. UV–vis absorption spectroscopy

UV–vis absorption spectra were recorded at 20 °C using a Jasco V-530 UV-vis spectrophotometer equipped with a 1 cm pathlength cell. The conditions were as follows: scanning rate: 100 nm min^{-1}, data pitch: 0.5 nm, and bandwidth: 2 nm. Titrations of miR-26b-5p [2.5 μM] were performed by adding increasing amounts of porphyrin. Generally, the porphyrins interacting with other molecules, form complexes which exhibit kinetic inertness; therefore, it is possible to perform UV titration to obtain information on the stoichiometry of these complexes. By plotting the Soret band absorbance *vs.* [porphyrin]/[miRNA], it is possible to reveal straight lines with different slopes; the change of the slope indicates the variation of the complex stoichiometry. Each straight line indicates the presence of a supramolecular species in solution, which is stable, inert and not in equilibrium with the others, and then it is characterized by a specific molar extinction coefficient.[33] Conversely, a unique straight line plot will appear all over the titration experiment if all the complexes formed are in equilibrium each other or in case the aggregation state of the molecule does not change (as well as observed in the case of porphyrin alone in buffer solution). The titrations were terminated when the straight line slope results are similar to those obtained by the titrations of the porphyrins alone in buffer solution. Break points are found where the titration line displays at least a 10% slope variation.

2.4. Fluorescence spectroscopy and resonance light scattering (RLS)

Fluorescence emission spectra and RLS were recorded using a Fluorolog FL-11 Jobin Yvon Horiba. Each experiment was carried out at 20 °C with a 1 cm quartz cuvette. For fluorescence measurements the following parameters were used: emission range of 550–800 nm, increment of 1.0 nm, averaging time of 0.1 s, one scan, and 2.5 nm slits both for excitation and emission. The excitation wavelength (λ_{ex}) was chosen taking into account the isosbestic points detected in the UV titrations for each porphyrin used: H2T4 (λ_{ex} = 430 nm); ZnT4 (λ_{ex} = 450 nm); H2TCPPSpm4 (λ_{ex} = 420 nm); ZnTCPPSpm4 (λ_{ex} = 450 nm).

3. Results and discussion

3.1. miR-26b-5p adopts well-defined structures in solution

First, to evaluate if the miR-26b-5p sequence adopts well-defined secondary structures (*e.g.* hairpins and/or self-dimers) or random conformations, we performed ECD measurements at different strand concentrations (0.7 μM, 2.8 μM and 10 μM) in PBS buffer at pH = 7.4 (Fig. 2(a)). For single stranded sequences in random conformations, the intensity of the signal is expected to be close to few millidegrees[11] In contrast, in the UV region between 300 nm and 220 nm, the ECD signal

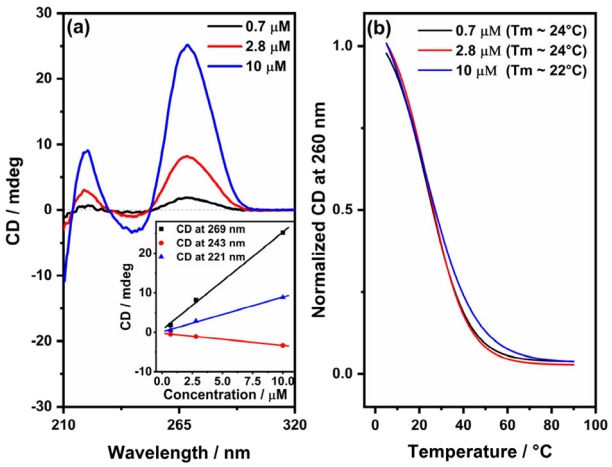

Fig. 2 (a) ECD spectra of miR-26b-5p in 10 mM PBS ([KCl], 2.7 mM; [NaCl], 137 mM; pH, 7.4) (0.7 μM, black curve; 2.8 μM, red curve; 10 μM, blue curve). Inset: a plot of the concentration of miR-26b-5p *vs.* the CD signal at 269 nm (black squares), 243 nm (blue triangles) and 221 nm (red circles). (b) ECD melting curves normalized to the [0,1] of miR-26b-5p in 10 mM PBS, pH = 7.4 (0.7 μM, black curve; 2.8 μM, red curve; 10 μM, blue curve).

of miR-26b-5p (at all the investigated concentrations) is quite structured and shows an intense band at around 270 nm, a less intense negative band at around 240 nm and a band at ~220 nm, suggesting that the sequence is not in a random conformation. Indeed, the ECD spectrum is similar to that of A-form RNA, indicating that the sequence is most likely folded in ordered secondary structures (*e.g.* self-dimers or hairpins). In addition, the intensity of the CD bands increases linearly with the concentration of the sequence (Fig. 2(a), inset), suggesting that the sequence does not change the conformations adopted in the concentration range investigated.

Second, we performed ECD melting experiments by monitoring the variation of the ECD signal at 260 nm in the range of 5–90 °C at different strand concentrations (0.7 μM, 2.8 μM and 10 μM) in PBS buffer (Fig. 2(b)). In general, for a solution containing nucleic acid sequences, two possible situations are possible. The first one, in which the nucleobases are not involved in hydrogen bonds and a temperature increase causes "only" the breaking of π–π interactions (in the case of highly structured single strands). In this case, the ECD intensity will decrease linearly upon increasing the temperature together with the smooth loss of base stacking. The second scenario, in which the nucleobases form either "internal" (*e.g.* hairpins) and/or "external" (*e.g.* duplexes) base-pairing, in which a temperature increase causes breaking of hydrogen bonds and a consequent "melting" of base–base coupling, leading to a net transition in the intensity–temperature graph (*i.e.* a sharp decrease of the ECD intensity), which is centered at the temperature where 50% of denaturation occurs (T_m).[11] Altogether, the loss of ordered structure by heating causes ECD changes which, monitored at a fixed wavelength as a function of temperature, allow us to estimate the stability of secondary structures. The melting curves showed a clear transition for this sequence, confirming that this sequence adopts well-defined folded structures.

To better understand if miR-26b-5p adopts in solution preferentially one structure (*e.g.* hairpin) rather than another one (*e.g.* self-dimers), we performed melting experiments at different concentrations (0.7 μM, 2.8 μM, and 10 μM) and for each one we recorded the melting temperature (T_m) (Fig. 2(b)). These experiments are very useful because monomolecular transitions (*e.g.* those associated with the unfolding of hairpins) are virtually independent of the strand concentration, while transitions with higher molecularities, as those associated with the dissociation of self-dimers, exhibit a significant dependence on the sample concentration. The obtained melting temperatures do not display significant differences among the concentrations investigated and for this reason, we speculated that this sequence is mostly folded in hairpins. In this context, we also predicted the possible hairpin structures using web tools like mFOLD[34] and RNAstructure,[35] providing additional support to our hypothesis (Fig. S1†).

3.2. Interaction of cationic H2T4 with miR-26b-5p

We first studied the interaction of H2T4 with miR-26b-5p by UV-vis absorption spectroscopy with the addition of increasing amounts of H2T4 (in the range of 0.5–19 μM) to miR-26b-5p (2.5 μM) in PBS buffer at pH = 7.4 (Fig. S1(a)†). In PBS buffer, H2T4 porphyrin displays the Soret band at 421 nm and other four less intense bands at 510, 550, 580 and 650 nm (Q bands) (black line, Fig. 3). After the addition of H2T4 up to 2.5 μM to a solution containing 2.5 μM miR-26b-5p, it is possible to observe a large bathochromic shift ($\Delta\lambda$ = 17 nm) and a hypochromic effect (~40%) of the porphyrin Soret band (red line, Fig. 3), suggesting a significant perturbation in the porphyrin

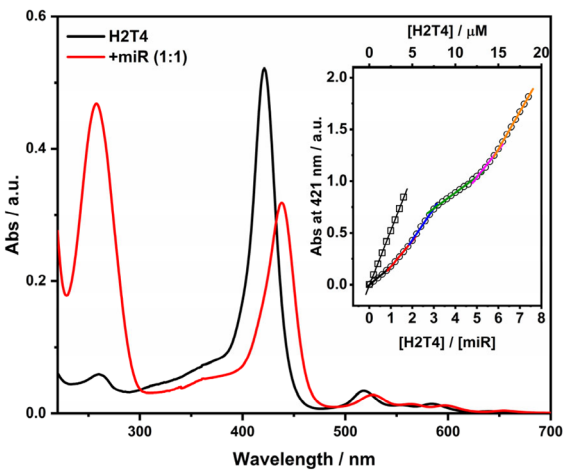

Fig. 3 Absorption spectra of H2T4 [2.5 μM] in 10 mM PBS ([KCl], 2.7 mM; [NaCl], 137 mM; pH, 7.4) (black curve) and in the presence of miR-26b-5p [2.5 μM] (red curve). Inset: a plot of absorbance at 421 nm *vs.* the concentration of H2T4 alone in PBS (squares) and *vs.* the [H2T4]/[miR-26b-5p] ratio (circles), lines with different colors indicate a different slope.

π electrons as a result of the binding to miRNA. In order to verify if the porphyrin binding mode with miR-26b-5p depends on the ratio of the two molecules, we have plotted the absorbance at 421 nm *versus* the [H2T4]/[miR] ratio. The plot shown in the inset of Fig. 3 shows five distinct break points, indicating the formation of five H2T4 : miR complexes (1 : 1, 2 : 1, 3 : 1, 5 : 1 and 6 : 1).

In particular, for complexes with porphyrin contents higher than 3 : 1, a strong hypochromic effect is observed, suggesting a stronger interaction among porphyrins with miRNA. Yet, after the formation of the 6 : 1 complex, further addition of H2T4 has no effect on the slope of the straight line (inset Fig. 3, orange line), which became almost identical to that one obtained for H2T4 alone in buffer solution (the inset in Fig. 3, black line). These results indicate that the formation of an H2T4/miR-26b-5p complex takes place up to a 6 : 1 ratio. Lastly, the second derivatives of the absorption spectrum of H2T4/miRNA complexes (Fig. S1(b)†) show that at the 5 : 1 ratio the band at around 420 nm is predominant, indicating that further addition of H2T4 does not interact with the H2T4/miRNA complexes.

As reported in the literature, the large bathochromic shift ($\Delta\lambda$ = 17 nm) and the strong hypochromic effect (~40%) of the porphyrin Soret band are ascribed to the intercalation of the ligand between two bases. However as mentioned above, mature miRNAs are short sequences and even if arranged in some secondary structures, the intercalation of porphyrin could be unlikely. Therefore, weak aggregation of porphyrins onto the miRNA structure could occur. In this context, the formation of dimers (two porphyrins interacting in a face-to-face mode between two miRNA structures in a fascinating way) cannot be excluded.

The emission spectrum of H2T4 (black line, Fig. 4(a)) displays a large broad band from 630 nm to 780 nm, which is mainly due to the coupling of the first excited state S1 with a nearby charge transfer state (CT) from the porphyrin core to the pyridinium group; the coupling is favored in high polarity solvents and can be assisted by the high degree of rotational flexibility of the *N*-methylpyridinium groups.[36] However, in the presence of miRNA (red line, Fig. 4(a)), it is possible to observe a change both in the fluorescence intensity and shape of the emission spectrum, confirming the interaction between the porphyrin and the miRNA. Indeed, the broad emission of H2T4, after the interaction with miRNA, is split into two peaks of Q(0, 0) and Q(0, 1) bands with emission maxima at around 660 and 730 nm (red line, Fig. 4(a)). This effect might be caused by the changes in the dielectric of the solvation sphere associated with the porphyrin, in fact generally the complex formation of H2T4 with nucleotides results in dielectric changes by reducing the accessibility of water molecules to the π orbitals of the porphyrin.[37] In addition, when the pyridinium groups stuck, the charge transfer effect is decreased, increasing the splitting effect of the broad emission band due to the reduction of rotational flexibility of the *N*-methylpyridinium groups. These two effects brought by binding with miRNA render the electronic S1–CT mixing less effective, causing the splitting of Q(0, 0) and Q(0, 1) bands. At the 3 : 1 (H2T4 : miR-26b-5p) ratio, the two emission bands become less resolved (Fig. S2†), suggesting some changes in the excited state of the porphyrin that could be ascribed to the formation of other H2T4 : miR-26b-5p complexes, in accordance with the absorbance data in which at this ratio an evident break point is displayed. The interaction with miR-26b-5p was also confirmed by resonance light scattering measurements (Fig. S3†). The RLS intensity of H2T4 alone is low and does not increase with increasing porphyrin concentrations (Fig. 4(b)), indicating the absence of aggregation in buffer solution, whereas the titration of miR-26b-5p with increasing amounts of H2T4 shows a strong enhancement in light scattering intensity when the concentration of H2T4 is 6.5 μM. Then the RLS intensity increases linearly after the addition of more H2T4 up to 10 μM (Fig. 4(b)), after that no enhancement is observed. The RLS results suggest that porphyrins are electronically coupled to miR-26b-5p up to the 4 : 1 (H2T4 : miR-26b-5p) ratio, whereas after the 4 : 1 ratio, the RLS intensity does not increase anymore, suggesting that other well-ordered H2T4 : miR-26b-5p complexes are not formed. However these data do not exclude the formation of other H2T4 : miR-26b-5p complexes at a higher ratio as suggested by the UV data. In addition, the enhancement of RLS intensity up to the H2T4 : miR-26b-5p ratio of 4 : 1 can be ascribed to the formation of well-ordered aggregates formed by porphyrins onto the miRNA structure rather than the aggregation phenomenon of porphyrins alone. The RLS and UV-vis data support our hypothesis of miR-assisted porphyrin self-aggregation, which leads to strong electronic communication between individual porphyrins in the assembly arranged as J-aggregates. The low intensity of the RLS signal at H2T4 : miR-26b-5p ratios of 1 : 1 and 2 : 1 could be ascribed to the low sensibility of the RLS technique to detect short aggregates, like dimers, which cannot be excluded as reported for the UV data.

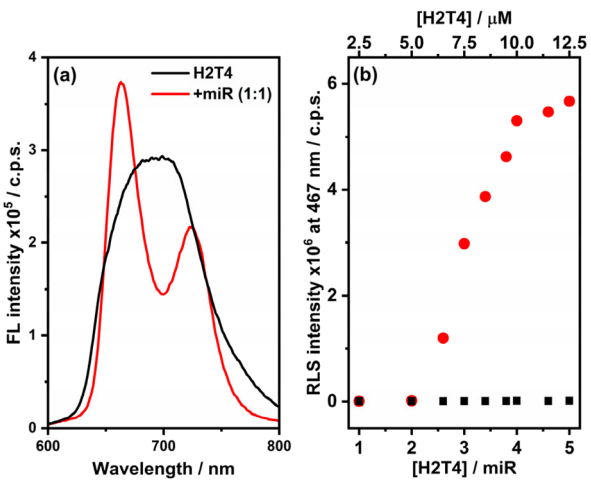

Fig. 4 (a) Emission spectra of H2T4 [2.5 μM] in 10 mM PBS ([KCl], 2.7 mM; [NaCl], 137 mM; pH, 7.4) (black curve) and in the presence of miR-26b-5p [2.5 μM] (red curve). (b) Plot of the intensity of the RLS signal at 467 nm *vs.* the [H2T4]/[miR-26b-5p] ratio (red circles) and *vs.* the concentration of [H2T4] alone in PBS (black squares).

Circular dichroism titrations with increasing amounts of H2T4 were performed. The CD signal of miR-26b-5p alone in solution in the UV region between 300 nm and 220 nm (black line, Fig. 5) shows an intense positive band at around 270 nm and a less intense negative band at around 240 nm, suggesting that the sequence is not in a random conformation. Upon increasing the addition of H2T4, the intense positive band decreased in intensity, suggesting a modification in the secondary structures of the miRNA. This observation indicates that the porphyrin may be unwinding the oligonucleotide structure. The region between 500 nm and 400 nm is highly diagnostic to differentiate the type of binding of an achiral porphyrin with polynucleotides; despite the fact that many ligands are achiral and optically inactive, they can acquire ICD signals when they interact with nucleic acids.[38] The presence of an ICD signal in the achiral ligand's absorption bands indicates that the ligand interacts with nucleic acids. In particular, very weak bisignate CD signals in the porphyrin Soret band at the 1 : 1 and 2 : 1 (H2T4 : miR-26b-5p) ratios are detected (Fig. 5). The bisignate CD signals indicate that electronic communication at least between two porphyrins occurs and in general is related to a substantial aggregation of porphyrins, but it could also be linked to an outer stacking of porphyrins onto the miRNA structure.[23] Therefore the bisignate ICD already detected at the 1 : 1 (H2T4 : miR-26b-5p) ratio indicates that electronic communication at least between two porphyrins occurs. However the UV data do not support the formation of porphyrin–porphyrin dimers since the plot of absorption intensity *vs.* the H2T4 : miRNA ratio shows five distinct break points, indicating the formation of five H2T4 : miR complexes (1 : 1, 2 : 1, 3 : 1, 5 : 1 and 6 : 1). Therefore, we suppose the formation of the porphyrin dimer with each porphyrin interacting with one miRNA sequence, whereas after the 3 : 1 ratio, the intensity of the bisignate signal drastically increases. It is conceivable to speculate that increasing the concentration of H2T4, especially after the 3 : 1 ratio, triggers porphyrin aggregation onto the miRNA structure, resulting in a stronger bisignate ICD signal, in accordance with the spectroscopic data shown previously.

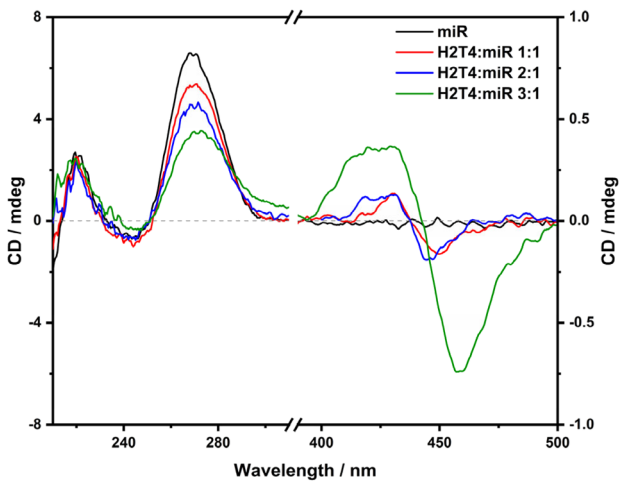

Fig. 5 ECD spectra of miR-26b-5p [2.5 μM] in 10 mM PBS ([KCl], 2.7 mM; [NaCl], 137 mM; pH, 7.4) (black curve) and in the presence of increasing amounts of H2T4 (2.5 μM, red curve; 5 μM, blue curve; 7.5 μM, green curve).

The several spectroscopic techniques used demonstrate that until the 3 : 1 (H2T4 : miR) ratio, there is a specific type of interaction involving the formation of a dimer of porphyrins with each porphyrin interacting with one miRNA sequence. The ratio of these complexes involving dimers should be 2 : 2 and 4 : 2 (H2T4 : miR) ratio however for the UV or RLS techniques those ratio are the same of 1 : 1 and 2 : 1 complexes. Indeed, the pronounced hypochromic effect in the absorption spectra, accompanied by two resolved bands in the emission spectrum, confirm that porphyrins are involved in a specific interaction. The lack of an increase in RLS intensity also excludes the possibility of strong aggregation, offering further confirmation of weak aggregation or dimer formation between two porphyrins and two miRNA molecules, as evidenced also by the weak bisignate-induced circular dichroism (ICD) signal. From the 3 : 1 ratio, instead, an aggregation of porphyrins onto the miRNA structure becomes predominant. This is indicated by the fluorescence bands becoming less resolved, an increase in RLS, and the enhancement of the bisignate in the ICD spectra, also in this case it is not possible to exclude the formation of dimers at the 6 : 2 (H2T4 : miR) ratio.

3.3. Interaction of cationic ZnT4 with miR-26b-5p

Second, we studied the interaction of the zinc(II) derivative of meso-tetrakis(4-*N*-methylpyridyl) porphyrin (ZnT4) with miR-26b-5p by using the same spectroscopic techniques used for the interaction of H2T4 with miR-26b-5p. UV-vis titrations with increasing amounts of ZnT4 (in the range of 0.5–12.5 μM) were performed in PBS buffer. The UV–vis absorption spectrum of ZnT4 (2.5 μM) in the absence of miRNA (black line, Fig. 6(a)) showed the Soret band at 436 nm and other two Q bands at 565 and 610 nm, respectively, whereas the presence of miR-26b-5p (2.5 μM) led to a red shift in the Soret band to 443 nm ($\Delta\lambda$ = 7 nm) and ~27% hypochromicity (% H) (red line, Fig. 6(a)). We have reported the absorbance variation at 436 nm *versus* the [ZnT4]/[miR-26b-5p] ratio (Fig. 6(a), inset), conversely to what is observed with H2T4; in this case, except for the first weak break point at the 1 : 1 (ZnT4 : miR) ratio, no others evident break points are shown, suggesting that the central metal (Zn) plays a crucial role in the interaction with miRNA, avoiding the formation of different types of binding modes. As suggested by the low bathochromicity and the slight hypochromicity, a very weak interaction occurred in comparison with the interaction between the H2T4 porphyrin and the miR sequence.

Both emission spectra (Fig. 6(b)) of ZnT4 porphyrin alone in PBS (black line) and in the presence of miRNA-26b-5p (red line) displayed two not well resolved bands at around 630 nm and 670 nm, and no significant differences in the intensity and shape are observed, confirming that a weak interaction occurred between ZnT4 and the miRNA.

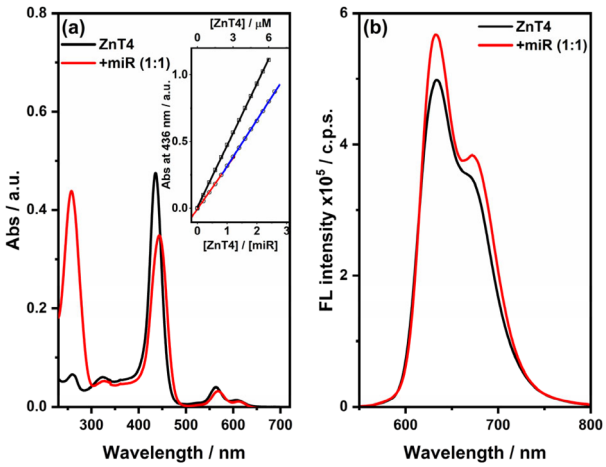

Fig. 6 (a) Absorption spectra of ZnT4 [2.5 μM] in 10 mM PBS ([KCl], 2.7 mM; [NaCl], 137 mM; pH, 7.4) (black curve) and in the presence of miR-26b-5p [2.5 μM] (red curve). Inset: a plot of absorbance at 436 nm *vs.* the concentration of ZnT4 alone in PBS (squares) and *vs.* the [ZnT4]/[miR-26b-5p] ratio (circles), lines with different colors indicate a different slope. (b) Emission spectra of ZnT4 [2.5 μM] in 10 mM PBS ([KCl], 2.7 mM; [NaCl], 137 mM; pH, 7.4) (black curve) and in the presence of miR-26b-5p [2.5 μM] (red curve).

Also, the RLS titration with increasing amounts of ZnT4 confirmed the absence of specific interaction with miRNA, indeed as shown in the RLS spectra (Fig. S5†), there is no enhancement in light scattering and this corroborate the hypothesis that porphyrins are not electronically coupled to the miRNA.

Circular dichroism titration performed with increasing amounts of ZnT4 (Fig. 7) displayed a slight modification of the miR-26b-5p signal at around 270 nm, indeed the intense positive band decreased slightly in intensity, proposing a lower destabilization of the miRNA in comparison with that of H2T4. Although the previous spectroscopic techniques suggested a very weak interaction between ZnT4 and the miRNA, a weak negative induced CD (ICD) signal appears at around 460 nm, and its intensity decreases with increasing ZnT4 concentration. Normally, a negative induced signal indicates the intercalation of the porphyrin within the base stacking of the oligonucleotide. However, ZnT4 is a penta-coordinated planar porphyrin within an axially coordinated water molecule, which should prevent intercalation between nucleobases; further intercalation generally results in a stronger bathochromic shift ($\Delta\lambda \geq 15$ nm) and more marked hypochromism (H ≥ 35%) in the absorption spectra than our results.[23] Therefore, it is more plausible that the negative ICD signal is due to a pseudo-intercalation of the ZnT4 porphyrin to the final sections of the miRNA sequence close to the 5′ and 3′ ends, respectively. Indeed, the final nucleotides are not involved in a base pairing and consequently they are more available to interact *via* stacking interactions with ligands having aromatic moieties.

3.4. Interaction of H2TCPPSpm4 with miR-26b-5p

Successively, meso-tetrakis(4-carboxyphenylspermine) porphyrin, H2TCPPSpm4, was used to characterize the interaction with miR-26b-5p to evaluate the contribution of the spermine arms which, under physiological conditions, have at least the most external amino groups positively charged.[26] The UV–vis absorption spectrum of H2TCPPSpm4 (2.5 μM) in the absence of miRNA (black line, Fig. 8) displayed the Soret band at 414 nm and other four less intense Q bands from 520 to 650 nm. However, the presence of miR-26b-5p (2.5 μM) produced a Soret band shift from 414 nm to 426 nm ($\Delta\lambda$ = 12 nm) and ~40% hypochromicity (red line, Fig. 8), indicating strong interactions between the π-system of porphyrin and the miRNA

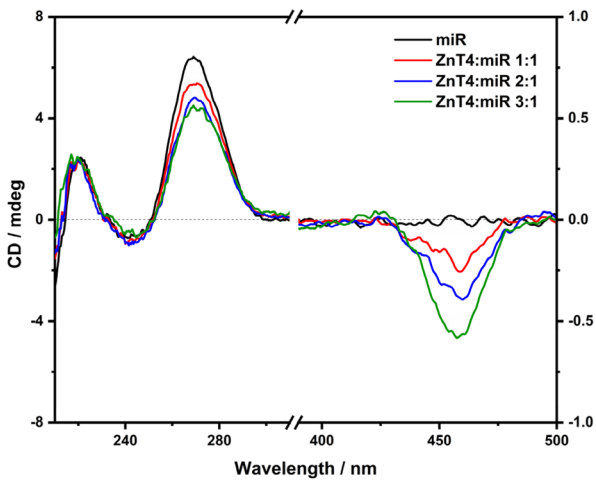

Fig. 7 ECD spectra of miR-26b-5p [2.5 μM] in 10 mM PBS ([KCl], 2.7 mM; [NaCl], 137 mM; pH, 7.4) (black curve) and in the presence of increasing amounts of ZnT4 (2.5 μM, red curve; 5 μM, blue curve; 7.5 μM, green curve).

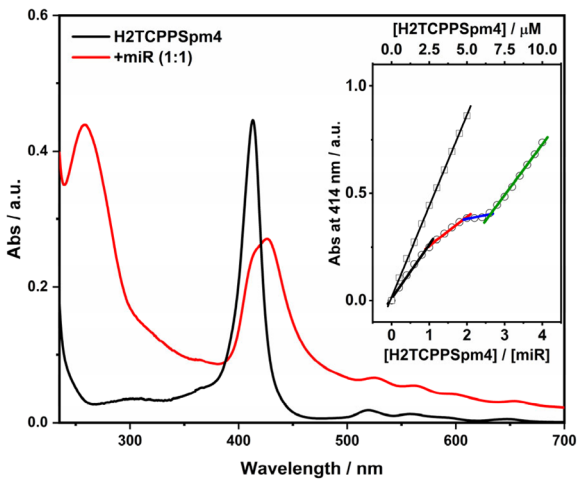

Fig. 8 Absorption spectra of H2TCPPSpm4 [2.5 μM] in 10 mM PBS ([KCl], 2.7 mM; [NaCl], 137 mM; pH, 7.4) (black curve) and in the presence of miR-26b-5p [2.5 μM] (red curve). Inset: a plot of absorbance at 414 nm *vs.* the concentration of H2TCPPSpm4 alone in PBS (squares) and *vs.* the [H2TCPPSpm4]/[miR-26b-5p] ratio (circles), lines with different colors indicate a different slope.

sequence, producing a similar behaviour to the interaction with H2T4.

Also, in this case we plotted the absorbance variation at 414 nm *versus* the [H2TCPPSpm4]/[miR-26b-5p] ratio (Fig. 8, inset).

At 1 : 1 and 2 : 1 (H2TCPPSpm4 : miR) ratios, two clear break points are displayed, then the absorbance does not increase until the 3 : 1 ratio and after that the slope of absorbance at 414 nm remains constant, demonstrating that the porphyrin is free in solution and it is no longer interacting with the oligonucleotide structure (inset Fig. 8, green line). Unlike the interaction with H2T4, which led to the formation of complexes with stoichiometry up to a 6 : 1 ratio (Fig. 3, inset), in this case H2TCPPSpm4 interacts with miRNA until the 3 : 1 ratio; this is ascribable to the bigger dimension of the molecule which bears four spermine arms, which hinder the possibility to form a complex with higher binding stoichiometry.

For the H2TCPPSpm4 porphyrin, as well as H2T4, the emission spectrum is formed by the initial excited state, S1, and the charge transfer state (CT) between the porphyrin core and its substituents at the meso-position, which in this case are formed by the carboxyphenylspermine groups. Polar solvents or the restriction of peripheral substituents can cause fluorescence quenching because of the coupling of these two states (S1–CT).

The emission spectrum of H2TCPPSpm4 alone in buffer solution (black curve, Fig. 9(a)) produced a broad peak centered at around 645 nm and a second band at around 700 nm. Noteworthily, from 5 μM concentration, the peak at 645 nm becomes larger and the maximum is red shifted ($\Delta\lambda \sim 5$ nm) (Fig. S7(a)†). To better understand the origin of this shift, we plotted the second derivatives of the absorption spectra at 1 μM and 5 μM concentrations of H2TCPPSpm4, respectively (Fig. S7(b)†). In the derivative plot (Fig. S7(b),† inset) at the concentration of 5 μM, a shoulder at around 405 nm appeared, and it became more pronounced at higher concentrations (data not shown). These results suggest that at a low concentration, H2TCPPSpm4 porphyrin is free in solution, while increasing the concentration triggers porphyrin aggregation which can explain the red-shift of the peak at around 645 nm in the emission spectra. The presence of miR-26b-5p (red line, Fig. 9(a)) led to a large decrease in fluorescence intensity and a red shift of 10 and 15 nm for the 650 and 700 nm peaks, respectively. The significant quenching of the fluorescence could be attributed to the close contacts between porphyrins and miRNA, as well as the self-association of porphyrin supported by the miRNA backbone. Emission spectra at 1 : 1 and 2 : 1 (H2TCPPSpm4 : miR) ratios are sharper and better resolved, proposing restriction in the rotation of the spermine arms upon interacting with the miRNA structure. At 3 : 1 and 4 : 1 ratios (Fig. S8†), the quenching becomes less intense and the emission spectra resembled to the spectra of the porphyrin alone in solution, implying that after the 2 : 1 ratio, porphyrins are no longer interacting, in accordance with the absorption data.

H2TCPPSpm4 alone exhibited a low RLS intensity (black squares, Fig. 9(b)), indicating that strong and ordered aggregation does not occur, whereas the titration of miR with increasing amounts of H2TCPPSpm4 led to an increase of the RLS intensity until the ~2 : 1 (H2TCPPSpm4 : miR) ratio (red circles, Fig. 9(b) and S9†), proposing an aggregation phenomenon with strong electronic communications among porphyrins arranged as J-aggregates on the miRNA structure. Increasing addition of porphyrin leads to a slight decrease of the RLS intensity, indicating that further addition does not form a complex with higher binding stoichiometry, in line with the UV-vis data.

The circular dichroism spectrum of miR-26b-5p with increasing amounts of H2TCPPSpm4 (Fig. 10) exhibited a strong reduction of the band at 270 nm, which could be explained by the preferential binding of porphyrins to single-stranded miRNA, which penalizes the formation of secondary structures by hydrogen base pairing. In particular, after the 2 : 1 (H2TCPPSpm4 : miR) ratio, the CD signal is close to few millidegrees, suggesting that the nucleobases are not involved in hydrogen bonds and the sequence is mainly in random single strands. A weak and negative ICD signal appeared in the Soret region, as also described previously, a negative induced signal suggests intercalation of the porphyrin within the base stacking of the oligonucleotide. However, it is remarkable to remember that the ICD signal arises from the chiral distortion of the porphyrin symmetry and/or intermolecular exciton coupling between at least two chiral well-oriented chromophores (porphyrin–porphyrin or porphyrin–nucleobase) and after the 2 : 1 ratio, the ICD signal disappeared, proposing that increasing porphyrin concentration induces the random conformations of the oligonucleotide structure, suggesting the external binding of the porphyrin onto the miRNA structure.

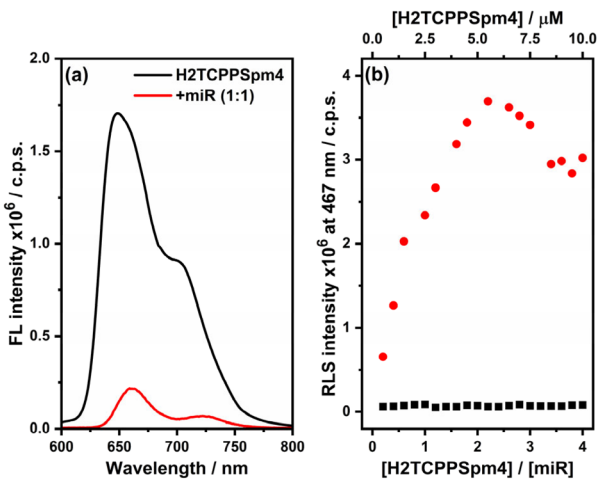

Fig. 9 (a) Emission spectra of H2TCPPSpm4 [2.5 μM] in 10 mM PBS ([KCl], 2.7 mM; [NaCl], 137 mM; pH, 7.4) (black curve) and in the presence of miR-26b-5p [2.5 μM] (red curve). (b) Plot of the intensity of the H2TCPPSpm4 RLS signal at 467 nm *vs.* the concentration of [H2TCPPSpm4] in the presence of miR-26b-5p (red circles) and alone in PBS (black squares).

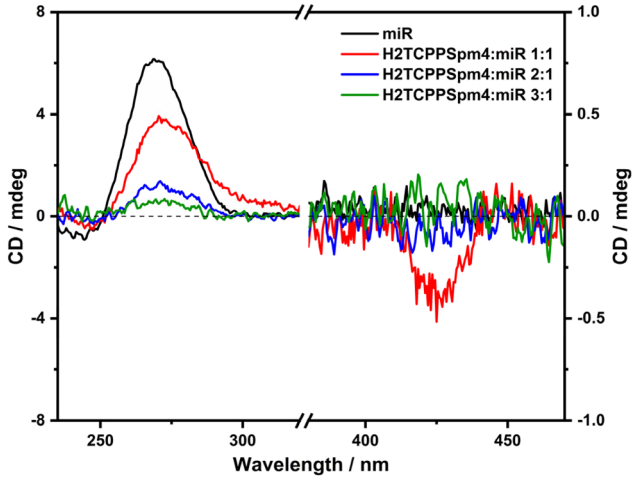

Fig. 10 ECD spectra of miR-26b-5p [2.5 μM] in 10 mM PBS ([KCl], 2.7 mM; [NaCl], 137 mM; pH, 7.4) (black curve) and in the presence of increasing amounts of H2TCPPSpm4 (2.5 μM, red curve; 5 μM, blue curve; 7.5 μM, green curve).

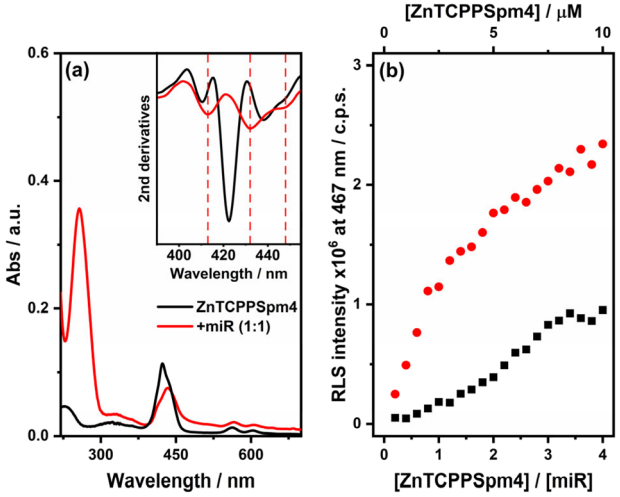

Fig. 11 (a) Absorption spectra of ZnTCPPSpm4 [2.5 μM] in 10 mM PBS ([KCl], 2.7 mM; [NaCl], 137 mM; pH, 7.4) (black curve) and in the presence of miR-26b-5p [2.5 μM] (red curve). Inset: 2nd derivatives of the UV-vis spectra. (b) Plot of the intensity of the RLS signal at 467 nm *vs.* the [ZnTCPPSpm4]/[miR-26b-5p] ratio (red circles) and *vs.* the concentration of [ZnTCPPSpm4] alone in PBS (black squares).

In conclusion, H2TCPPSpm4 destabilize the secondary structures of miR stronger than the H2T4 porphyrin, suggesting that the four spermine pendants have a predominant effect to disrupt the hydrogen base–pair interactions of the miR structures, causing its conformational change.

3.5. Interaction of ZnTCPPSpm4 with miR-26b-5p

In a recent work[30] it was reported that the ZnTCPPSpm4 porphyrin does not aggregate in 10 mM lithium cacodylate buffer (pH, 7.2; 5 mM KCl; 95 mM LiCl) up to the porphyrin concentration of 40 μM, showing the Soret band of the monomeric form at 424 nm. However, differently from the other porphyrins described previously, ZnTCPPSpm4, even at very low concentrations, tends to aggregate in PBS solution as recently reported.[39] Indeed, the UV-vis titration in PBS of ZnTCPPSpm4 alone (in the range of 0.5–10 μM) revealed a broad and a not well resolved Soret band at around 423 nm with two different shoulders at around 410 nm and 440 nm (black line, Fig. 11(a)), indicating the coexistence of the porphyrin in the monomeric and aggregated forms, whereas the UV-vis titration with increasing amounts of ZnTCPPSpm4 in the presence of miRNA [2.5 μM] (Fig. S10(b)†) produced a broad band with the maximum at 434 nm and two shoulders at around 413 nm and 450 nm (red line, Fig. 11(a)), accompanied by extended hypochromicity.

As a result of the aggregation starting state of ZnTCPPSpm4, it is not possible to perform stoichiometric analysis with miRNA. However, it is possible to observe that in the presence of miRNA, all the absorption bands of ZnTCPPSpm4 are red shifted (inset, Fig. 11(a)), suggesting an interaction between porphyrin aggregates and the miRNA structure.

Emission measurements of ZnTCPPSpm4 with and without miRNA did not produce detectable fluorescence spectra in both cases, also at higher porphyrin concentration. This is due to the specific assembly of porphyrin aggregates with the miRNA's phosphate backbone and phosphate molecules, respectively, which causes quenching of the fluorescence emission.[39]

Also, the RLS of ZnTCPPSpm4 alone (black squares, Fig. 11(b)) confirms the self-aggregation phenomenon. Indeed, the RLS intensity slightly increases with increasing porphyrin concentration. However, in the presence of miRNA (red circles, Fig. 11(b) and S11†) the RLS intensity is enhanced, proposing a stronger and well-ordered communication among porphyrins onto the miRNA sequence. The spectroscopic evidence advises the idea that the presence of ordered templates, such as the miRNA structure, induces better organization of the porphyrin aggregates.

Conversely from what observed with other porphyrins used previously, circular dichroism with increasing amounts of ZnTCPPSpm4 (Fig. 12) did not produce significant changes in the miRNA CD signal at around 270 nm, indicating that this porphyrin does not destabilize and modify the secondary structures adopted by the miRNA. In the Soret absorption region, a positive bisignate ICD signal is detected (Fig. 12). This signal is opposite to the bisignate ICD observed for H2T4 (Fig. 5), suggesting that the aggregates formed have a different orientation relative to the microRNA (miR) assembly when interacting with H2T4. The low intensity of this ICD signal can be attributed to the low absorbance shown in the UV-vis spectra for these aggregates and/or to a very weak interaction between ZnTCPPSpm4 and the miRNA.

3.6. ECD melting and apparent association constants

To support the hypothesis that ZnTCPPSpm4 does not affect the stability of the miRNA and to verify how other porphyrins modulate its stability, we performed ECD melting

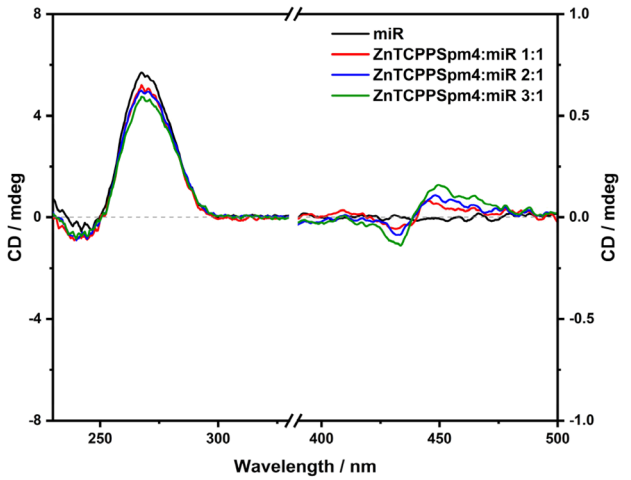

Fig. 12 ECD spectra of miR-26b-5p [2.5 μM] in 10 mM PBS ([KCl], 2.7 mM; [NaCl], 137 mM; pH, 7.4) (black curve) and in the presence of increasing amounts of ZnTCPPSpm4 (2.5 μM, red curve; 5 μM, blue curve; 7.5 μM, green curve).

experiments at [porphyrin]/[miR] 1 : 1 (Fig. S12(a)†) and 3 : 1 ratios (Fig. S12(b)†).

As we expected, miR-26b-5p in the presence of 2.5 μM and 7.5 μM ZnTCPPSpm4 exhibited a melting temperature (T_m) of ~23 °C and ~26 °C, respectively. These temperatures are similar to the T_m of miRNA alone in solution (T_m ~ 24 °C), confirming that this porphyrin does not destabilize the microRNA's secondary structures. Other porphyrins used at the [porphyrin]/[miR] 1 : 1 ratio do not affect the stability of the miRNA, except for H2TCPPSpm4 which displayed a T_m of ~17 °C. Most notably, at the 3 : 1 ratio for H2T4 and H2TCPPSpm4, it is not possible to perform CD melting experiments due to the high porphyrin concentration, which almost completely unwound the miRNA structure, in line with spectroscopic data described previously. Consequently, the excessive noise in the CD signal precluded the acquisition of a reliable melting curve.

Finally, we estimated the binding constant between miR-26b-5p and each porphyrin based on their absorption data using eqn (1).[40] In this equation, 'ν' represents the number of moles of bound porphyrin per mole of the total miRNA, 'L' signifies the molar concentration of free porphyrin, 'n' denotes the number of consecutive lattice residues (or miRNA sites) that become inaccessible due to the binding of a single porphyrin molecule, and 'K_{app}' stands for the apparent association constant of porphyrin binding to a site on the nucleic acid. The values of 'ν' and 'L' required for this analysis were determined by using the Peacocke and Sherrett method (see the ESI† for details).[41]

$$\frac{\nu}{L} = K_{app}(1 - n\nu)\left(\frac{1 - n\nu}{1 - (n-1)\nu}\right)^{n-1} \quad (1)$$

In a typical linear Scatchard plot (Fig. S13(a), (c) and (d)†), the slope extrapolation corresponds to K_{app} according to eqn (1). Thus, our estimated K_{app} values are listed in Table 1.

Table 1 Apparent association constants (K_{app}) for H2T4, ZnT4 H2TCPPSpm4 and ZnTCPPSpm4 with miR-26b-5p obtained from the Scatchard plots (see the ESI† for details)

miRNA	Porphyrin	K_{app} M^{-1}
miR-26b-5p	H2T4	4.84×10^5
miR-26b-5p	ZnT4	1.57×10^5 [a]
miR-26b-5p	H2TCPPSpm4	3.21×10^5
miR-26b-5p	ZnTCPPSpm4	1.34×10^6

[a] See the ESI† for details.

As we expected, similar K_{app} values were obtained for H2T4 and H2TCPPSpm4, in contrast, ZnT4 exhibited the lowest K_{app}, consistent with our spectroscopic results. Noteworthily, for ZnTCPPSpm4, higher K_{app} was found, indicating that the pre-organization of ZnTCPPSpm4 can enhance its affinity for miR-26b-5p.

4. Conclusions

In conclusion, we reported the supramolecular interaction between several achiral porphyrins and a mature miRNA. It was demonstrated that porphyrins can be used as chiroptical probes for miR-26b-5p and depending on their characteristics, different binding modes were observed, as evidenced by the different ICD signals produced in the Soret region. In particular, H2T4, up to the 2 : 1 ratio, appears capable of forming weak aggregations with the miRNA structure, forming dimers between porphyrins and miRNA molecules. After this ratio, H2T4 aggregates onto the miRNA structure *via* electrostatic interactions with the phosphate backbone, whereas the presence of one water molecule as the axial ligand of Zn in the porphyrin avoids aggregation in favor of pseudo-intercalation. For H2TCPPSpm4, a negative ICD signal is displayed until the 1 : 1 ratio; at a higher porphyrin concentration, it disappeared, suggesting that spermine arms are able to disrupt the miRNA's hydrogen base pairing, penalizing the formation of well-ordered secondary structures. For ZnTCPPSpm4, a pre-organized multi-porphyrinic system appears and then it interacts with the miRNA structure.

Lastly, CD-melting experiments demonstrated that the porphyrins used in this work do not affect the stability of the miRNA at the 1 : 1 ratio, excluding H2TCPPSpm4 that even at this low concentration showed a strong destabilizing behavior. Intriguingly at the 3 : 1 ratio, the unique porphyrin that does not destabilize the miRNA structure was ZnTCPPSpm4, which for this reason makes it the best candidate for further investigation and conformational studies on mature miRNA structures. The stronger destabilizing behavior observed for H2T4 and H2TCPPSpm4 may be associated with the fact that they do not pre-organize in solution; consequently the four positive charges at the meso-positions, as well as the aromatic core, are totally free to interact with the miRNA structures *via* electrostatic and stacking interactions, respectively. These porphyr-

ins, especially H2TCPPspm4, could be used as denaturing agents for mature miRNAs, deactivating in this way their biological function even at micromolar concentrations, making porphyrins potential drugs in connection with pathological contexts partially/totally caused by some miRNA upregulation.

The presence of Zn(II) at the central core of both porphyrins significantly varies their interaction with miRNA. Specifically, weaker interactions and a minor destabilizing effect were observed with ZnT4. However, the highest apparent association constant was obtained with ZnTCPPSpm4. This result suggests that the possibility to form ZnTCPPspm4 dimers in the presence of coordination bonds between the nitrogen atoms of the spermine pendant and the zinc atoms[39] avoids the destabilization of the miRNA structure. Therefore the contemporary presence of Zn(II) and spermine pendants stems a different effect with respect to that observed in the case when Zn(II) and spermine are in different molecules, as seen in the case of ZnT4 and H2TCPPspm4. This highlights the potential use of ZnTCPPspm4 as a chiroptical probe for miRNAs in spatial transcriptomics and single-cell analysis. In perspective, a better understanding of the miRNA structure, stability, and associated regulatory mechanisms should open up new opportunities to better understand their biological role and how messenger RNA targets are recognized.

Author contributions

Conceptualization: A. D. and R. P.; data curation: A. D., M. G. and G. T.; formal analysis: G. T. and M. G.; funding acquisition: A. D.; investigation: G. T.; methodology: A. D. and R. P.; project administration: A. D.; resource: A. D., C. M. G. and G. T.; supervision: A. D.; validation: G. T. and M. G.; visualization: A. D. and G. T; writing – original draft: G. T. and A. D.; writing – review and editing: R. P., S. A. and A. F.

Conflicts of interest

There are no conflicts to declare.

Acknowledgements

This research was funded by MUR PRIN 2017 project code: 2017YJMPZN-005 and PRIN 2022 project code: 2022R9WCZS; Programma Ricerca di Ateneo UNICT 2016-18 linea 1 e 2; Programma Ricerca di Ateneo UNICT 2020-2022 linea 2. Progetto "sAMpEI" Misura 2.51 PO FEAMP 2014-2020 – CUP: G67B18000260009.

References

1 R. Garzon, G. A. Calin and C. M. Croce, *Annu. Rev. Med.*, 2009, **60**, 167–179.
2 R. Schickel, B. Boyerinas, S. M. Park and M. E. Peter, *Oncogene*, 2008, **27**, 5959–5974.
3 V. Ambros, *Nature*, 2004, **431**, 350–355.
4 M. Acunzo, G. Romano, D. Wernicke and C. M. Croce, *Adv. Biol. Regul.*, 2015, **57**, 1–9.
5 C. Guay, E. Roggli, V. Nesca, C. Jacovetti and R. Regazzi, *Transl. Res.*, 2011, **157**, 253–264.
6 C. M. Croce, *Nat. Med.*, 2011, **17**, 935–936.
7 S. Gupta, S. Verma, S. Mantri, N. E. Berman and R. Sandhir, *Drug Dev. Res.*, 2015, **76**, 397–418.
8 R. Rupaimoole and F. J. Slack, *Nat. Rev. Drug Discovery*, 2017, **16**, 203–221.
9 M. M. Janas, B. Wang, A. S. Harris, M. Aguiar, J. M. Shaffer, Y. V. B. K. Subrahmanyam, M. A. Behlke, K. W. Wucherpfennig, S. P. Gygi, E. Gagnon and C. D. Novina, *RNA*, 2012, **18**, 2041–2055.
10 A. Belter, D. Gudanis, K. Rolle, M. Piwecka, Z. Gdaniec, M. Z. Naskret-Barciszewska and J. Barciszewski, *PLoS One*, 2014, **9**, e113848.
11 C. M. A. Gangemi, S. Alaimo, A. Pulvirenti, S. García-Viñuales, D. Milardi, A. P. Falanga, M. E. Fragalà, G. Oliviero, G. Piccialli, N. Borbone, A. Ferro, A. D'Urso, C. M. Croce and R. Purrello, *Sci. Rep.*, 2020, **10**, 1–11.
12 J. K. Choi, A. D'Urso and M. Balaz, *J. Inorg. Biochem.*, 2013, **127**, 1–6.
13 I. G. Occhiuto, M. Samperi, M. Trapani, G. De Luca, A. Romeo, R. F. Pasternack and L. M. Scolaro, *J. Inorg. Biochem.*, 2015, **153**, 361–366.
14 M. Balaz, M. De Napoli, A. E. Holmes, A. Mammana, K. Nakanishi, N. Berova and R. Purrello, *Angew. Chem., Int. Ed.*, 2005, **44**, 4006–4009.
15 H. Dill, B. Linder, A. Fehr and U. Fischer, *Genes Dev.*, 2012, **26**, 25–30.
16 J. Li, X. Li, X. Kong, Q. Luo, J. Zhang and L. Fang, *Int. J. Clin. Exp. Med.*, 2014, **7**, 558.
17 G. Duan, C. Ren, Y. Zhang and S. Feng, *Tumor Biol.*, 2015, **36**, 6201–6209.
18 F. Fan, J. Lu, W. Yu, Y. Zhang, S. Xu, L. Pang and B. Zhu, *Oncol. Lett.*, 2018, **15**, 386–392.
19 K. Wu, X. Y. Mu, J. T. Jiang, M. Y. Tan, R. J. Wang, W. J. Zhou, X. Wang, Y. Y. He, M. Q. Li and Z. H. Liu, *Oncol. Rep.*, 2018, **40**, 3523–3532.
20 K. Miyamoto, N. Seki, R. Matsushita, M. Yonemori, H. Yoshino, M. Nakagawa and H. Enokida, *Br. J. Cancer*, 2016, **115**, 354.
21 D. Wang, C. Liu, Y. Wang, W. Wang, K. Wang, X. Wu, Z. Li, C. Zhao, L. Li and L. Peng, *Cell Proliferation*, 2017, **50**, 1–12.
22 S. Absalon, D. M. Kochanek, V. Raghavan and A. M. Krichevsky, *J. Neurosci.*, 2013, **33**, 14645–14659.
23 K. E. Thomas and D. R. McMillin, *J. Phys. Chem. B*, 2001, **105**, 12628–12633.
24 R. F. Pasternack, E. J. Gibbs and J. J. Villafranca, *Biochemistry*, 1983, **22**, 2406–2414.
25 U. Sehlstedt, B. Nordén, S. K. Kim, P. Carter, J. Goodisman, J. C. Dabrowiak and J. F. Vollano, *Biochemistry*, 1994, **33**, 417–426.

26 C. M. A. Gangemi, R. Randazzo, M. E. Fragalà, G. A. Tomaselli, F. P. Ballistreri, A. Pappalardo, R. M. Toscano, G. T. Sfrazzetto, R. Purrello and A. D'Urso, *New J. Chem.*, 2015, **39**, 6722–6725.
27 C. E. Holbert, J. R. Foley, T. M. Stewart and R. A. Casero, *Int. J. Mol. Sci.*, 2022, **23**, 6798.
28 A. D'Urso, R. Randazzo, V. Rizzo, C. M. A. Gangemi, V. Romanucci, A. Zarrelli, G. A. Tomaselli, D. Milardi, N. Borbone, R. Purrello, G. Piccialli, G. di Fabio and G. Oliviero, *Phys. Chem. Chem. Phys.*, 2017, **19**, 17404–17410.
29 C. M. A. Gangemi, B. D'Agostino, R. Randazzo, M. Gaeta, M. E. Fragalà, R. Purrello and A. D'Urso, *J. Porphyrins Phthalocyanines*, 2018, **22**, 581–587.
30 N. C. Sabharwal, J. Chen, J. H. J. Lee, C. M. A. Gangemi, A. D'urso and L. A. Yatsunyk, *Int. J. Mol. Sci.*, 2018, **19**, 3686.
31 C. M. A. Gangemi, A. D'Urso, G. A. Tomaselli, N. Berova and R. Purrello, *J. Inorg. Biochem.*, 2017, **173**, 141–143.
32 O. Herrmann, S. H. Mehdi and D. A. Corsini, *Can. J. Chem.*, 1978, **56**, 1084–1087.
33 A. D'urso, M. E. Fragalà and R. Purrello, *Chem. Commun.*, 2012, **48**, 8165–8176.
34 M. Zuker, *Nucleic Acids Res.*, 2003, **31**, 3406–3415.
35 S. Bellaousov, J. S. Reuter, M. G. Seetin and D. H. Mathews, *Nucleic Acids Res.*, 2013, **41**, W471–W474.
36 F. J. Vergeldt, R. B. M. Koehorst, A. Van Hoek and T. J. Schaafsma, *J. Phys. Chem.*, 1995, **99**, 4397–4405.
37 G. A. Hembury, V. V. Borovkov and Y. Inoue, *Chem. Rev.*, 2008, **108**, 1–73.
38 R. F. Pasternack, *Chirality*, 2003, **15**, 329–332.
39 G. Travagliante, M. Gaeta, C. M. A. Gangemi, R. Purrello and A. D'Urso, *J. Porphyrins Phthalocyanines*, 2023, **27**, 509–516.
40 R. F. Pasternack, E. J. Gibbs and J. J. Villafranca, *Biochemistry*, 1983, **22**, 2406–2414.
41 A. R. Peacocke and J. N. H. Skerrett, *Trans. Faraday Soc.*, 1956, **52**, 261–279.